Optimum Launch Trajectories for the ATS-E Mission

OMER F. SPURLOCK* AND FRED TEREN†
NASA Lewis Research Center, Cleveland, Ohio

Optimum trajectories for the Applications Technology Satellite (ATS)-E mission are obtained. Analysis, procedure, and results are presented. The trajectories are numerically integrated from launch to insertion into the final orbit. As a result of a much smaller than optimum apogee motor, these trajectories, unlike conventional synchronous orbit trajectories, require noncircular parking orbits and large amounts of inclination reduction before the solid motor burn at apogee. Constraints on parking orbit perigee radius and duration are included.

Nomenclature

C = first integral of Euler-Lagrange equations, kg/sec
E = energy per unit mass, m²/sec²
e = eccentricity, N.D.
F = functional defined by Eq. (3), kg/sec
$\hat{f}$ = unit thrust direction, N.D.
$\mathbf{G}$ = gravity acceleration, m/sec²
G_m* = spherical earth gravity constant, m³/sec²
$\mathbf{G}_1,\mathbf{G}_2$ = components of oblate gravity acceleration, m/sec²
h = angular momentum/unit mass, m²/sec
J = functional to be minimized, kg
m = mass, kg
N = total number of stages, N.D.
p = semi-latus rectum, m
r,r_p = radius and perigee radius, respectively, m
S = variational switching function, N.D.
T = thrust, N
t = time, sec
v = velocity, m/sec
x = state variable
$\hat{z}$ = unit vector pointing at north pole, N.D.
β = mass flow rate, kg/sec
ϵ = jump factor
η = Lagrange multiplier, kg/sec
λ = Lagrange multiplier, kg-sec/m
μ = Lagrange multiplier, kg/m
σ = Lagrange multiplier, N.D.
ψ,φ = pitch and yaw attitude, respectively, deg

Superscripts

$\cdot$ = time derivative
$\hat{}$ = unit vector
f = final
o = initial

Subscripts

f = final
d = desired
i,j,k,l,m,n = stage numbers
o = initial
pk = parking orbit

Operators

$\cdot$ and $\mathbf{x}$ = dot and cross product, respectively
$d(\ )$ = differential
$\nabla_{\mathbf{x}}(\ )$ = gradient with respect to $\mathbf{x}$
$\partial(\ )/\partial(\ )$ = partial derivative

Presented as Paper 70-1051 at the AAS/AIAA Astrodynamics Conference, Santa Barbara, Calif., August 19–21, 1970; submitted September 18, 1970; revision received June 23, 1971.

Index Categories: Launch Vehicle and Missile Trajectories; Earth-Orbital Trajectories.

* Aerospace Engineer, Vehicle Performance Section, Advanced Systems Division. Member AIAA.

† Head, Vehicle Guidance Section, Advanced Systems Division.

Introduction

THE Applications Technology Satellite (ATS)-E mission is a circular synchronous equatorial orbit mission with an objective of advancing technology which may have application to future spacecraft. Spacecraft-oriented experiments on the ATS-E provide information on power supply and control systems, a gravity-gradient stabilization system, resistojet and ion micropound thrusters, and synchronous environment. Scientific-oriented experiments gather data on the particle (electron and proton) distribution and flux and the character of the electric and magnetic fields at synchronous altitude.

The launch vehicle for the ATS-E mission was an Atlas-Centaur and the solid apogee motor was a part of the spacecraft system. The apogee motor total impulse was sized for the early ATS missions on the Atlas-Agena launch vehicle, which has less payload capability than the Atlas-Centaur. The apogee motor, although smaller than optimum for the larger vehicle, remained unchanged.

For an optimally sized apogee motor, a conventional trajectory to circular synchronous equatorial orbit is near optimum, and consists of five consecutive phases as shown in Fig. 1. The first phase is an ascent from the launch site to a circular parking orbit. To maximize the mass in orbit, a 90° launch azimuth is used, which results in a parking orbit inclination equal to the launch site latitude. This inclination must be removed during the trajectory. The second phase is a coast arc to the proximity of the equator. In the third phase a small portion of the required plane change is removed with a second burn. Much more importantly, the second burn must place the vehicle in a transfer orbit whose apogee is over the equator and equal to synchronous altitude. The vehicle coasts to apogee in the fourth phase. The fifth phase consists of a final burn that removes the major portion of the inclination and circularizes the orbit. Intuitively, it seems reasonable that this conventional profile is near optimum if the burn and coast durations may be varied to maximize the mass at the end of each burn. However, if the total impulse of the final burn is fixed at less than the optimum value, the conventional trajectory must be modified to yield maximum payload to the final orbit. In particular, the parking orbit is noncircular, the perigee radius of the transfer orbit increases, and the second burn removes more than a minor part of the inclination. The optimization problem is to find the best combination of these changes and other less important ones to yield maximum payload to circular synchronous equatorial orbit.

Optimization of the conventional trajectory to circular synchronous equatorial orbit has been treated by several authors. Hoelker and Silber[1] present a detailed analysis of the conventional problem. Rider[2] considers the problem of changing the plane and also the radius of a circular orbit.

These and other similar studies treat the problem as one of changing the plane and radius of a circular orbit, ignoring the ascent to the first (parking) circular orbit. This is satisfactory for the conventional case. However, an unconventional trajectory is more complex since the parking orbit is in general noncircular. Therefore, the ascent must be included as part of the optimization problem, and a more sophisticated optimization procedure is required. Additionally, the references mentioned previously do not consider constraints which may alter the acceptability of a given trajectory, such as limitations on coast time or the minimum parking orbit perigee radius.

The problem of optimizing the trajectories to circular synchronous equatorial orbit may be considered as a multistage launch vehicle optimization, for which several analyses have been performed including one by the authors of this report.[3] For optimizing the unconventional trajectory, the analysis in Ref. 3 was expanded to three dimensions and also, to include a constraint on the parking orbit perigee radius. The perigee radius constraint must be included to limit aerodynamic heating on the spacecraft.

Analysis

Problem Description

The nonplanar characteristics of the ascent trajectory are shown in Fig. 2. The vehicle is launched at an azimuth of 90° in order to maximize the vehicle mass in parking orbit and to minimize the inclination of the parking orbit. The circular parking orbit altitude is as low as aerodynamic heating constraints will allow, usually about 165 to 185 km. The parking orbit coast time is usually about 15 min—the time required to coast from orbit insertion to the first equator crossing. The third phase places the vehicle in a transfer orbit whose apogee and perigee are over the equator. The apogee altitude is about equal to the required altitude for a circular synchronous orbit. The transfer orbit coast time is about $5\frac{1}{2}$ hr. The third impulse, the apogee burn, occurs at apogee of the transfer orbit. Apogee is designed to occur at the equator and at the proper altitude for injection into the final orbit. A small part of the inclination is removed by the second impulse with the remainder being removed by the apogee burn. In this conventional method, the final conditions at the end of each burn are known and the mass can easily be maximized progressively phase by phase if the second and third impulse sizes are unspecified.

Now suppose that the total impulse of the third burn is fixed. Then the transfer orbit must be constructed such that the ΔV available from the third impulse is exactly that required to place the vehicle in circular synchronous equatorial orbit. If the ΔV available from a fixed third total impulse is less than that required to circularize and equatorialize the orbit for the mass available from a conventional ascent and second impulse, then the trajectory to transfer orbit insertion must be altered to reduce the ΔV required of the third impulse. This can be done by reducing the required plane change and the ΔV required for circularization. For reasons described in the Procedure and Results section, the unconventional trajectory needed to reduce the ΔV required of the apogee motor varies in many respects from the conventional profile. The most dramatic changes are a noncircular parking orbit, nontrivial inclination reduction by the second impulse, and a significantly nonequatorial latitude for the second impulse. As is desired, the changes result in lowering the ΔV required of the fixed apogee motor. However, in this unconventional profile, the final conditions required at the end of the ascent and second impulse are unknown. They might be determined by varying those final conditions parametrically until the optimum is obtained. However, because of the number of variables, this process is clumsy and time consuming.

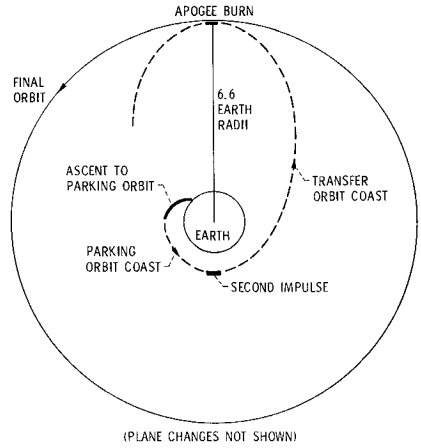

Fig. 1 Conventional trajectory to circular synchronous equatorial orbit.

Calculus of Variations Solution

A calculus of variations formulation was used to maximize the payload to circular synchronous equatorial orbit without resorting to a parametric search. The optimization of the atmospheric portion of the trajectory is omitted from the variational analysis since the steering is constrained by factors other than optimizing performance, such as aerodynamic loading and heating limitations. The analysis considers the problem from the point in the trajectory that the atmosphere can be neglected to insertion into the final orbit. In addition to optimizing the steering, the durations of any unspecified burns and coasts are optimized while maintaining the specified perigee radius of the parking orbit. The analysis is presented in Appendix A. It is derived in three dimensional rectangular coordinates in a manner similar to Ref. 4. The equations for optimum burn and coast duration are obtained from an analysis similar to that used by the authors in Ref. 3. It is necessary to extend the analysis to include an intermediate boundary condition which specifies the perigee radius of the parking orbit at the end of the ascent. Additionally, the oblate Earth model must be added to the variational analysis. The effect of oblateness is not negligible in trajectories to circular synchronous equatorial orbit. Trajectories to that orbit are long, minimally around six hours. Oblateness is the major perturbing force during most of a trajectory. Because of the large change in inclination required to perform the mission, any perturbation in the inclination, thus increasing or decreasing the amount of plane change required of the propulsion systems, affects the final mass and should be considered in the analysis.

The trajectories are numerically integrated to incorporate a nonimpulsive vehicle model and to include the effects of oblateness and small thrusts over long periods of time which cannot be conveniently treated impulsively.

The analysis presented in Appendix A requires the solution of a two-point boundary value problem. With a fixed apogee burn and parking orbit coast time, a minimum of eight final conditions with an equal number of initial conditions, must be satisfied.

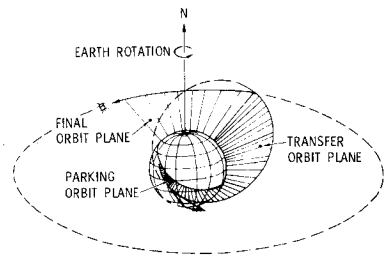

Fig. 2 Circular synchronous equatorial orbit ascent profile.

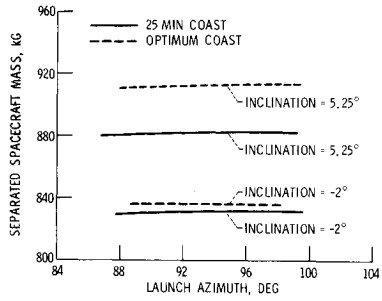

Fig. 3 Separated spacecraft mass as a function of launch azimuth.

Procedure and Results

A simple Newton Raphson iteration scheme was used to successfully solve the two-point boundary value problem with as many as twelve iteration variables. For further explanation of the iteration scheme, see Ref. 5.

The partial derivatives required for the iteration scheme were obtained by integrating the adjoint equations. These were obtained as in Ref. 4. Solutions were initially obtained by using a spherical earth model for the adjoint equations, but it was found that including the oblateness terms improved the convergence properties of the problems.

It was difficult to obtain solutions to these problems because of the high degree of nonlinearity of many of the derivatives, as well as the difficulty of guessing at the initial values of the thrust angle in pitch and yaw and their rates. A technique (described in Appendix B) was devised to systematically proceed from a simple, easily converged problem to the final solution. Other techniques, such as gradient methods, might avoid some of the difficulties associated with the Newton Raphson technique. However, the method described is convenient, straightforward, and adequate. After obtaining one solution, proceeding to others in the region of interest is not difficult.

The trajectory starts with a short vertical rise, followed by a rapid pitchover phase in the desired azimuth direction. The amount of pitchover determines the amount of lofting during the atmospheric portion of the trajectory. The remainder of the atmospheric phase (which is assumed to end at booster stage jettison), is flown with a near-zero angle of attack steering program (described in Ref. 5), to minimize vehicle heating and aerodynamic loads. The thrust direction is constrained to be parallel to the launch azimuth plane, which is established at launch.

Since the ATS-E spacecraft motor has a fixed propellant load, the trajectory must be designed such that the ΔV required at apogee of the transfer orbit is exactly that required to place the spacecraft in the desired final orbit. As mentioned earlier, the ATS-E motor is much smaller than optimum. The Atlas-Centaur can put more mass in a conventional transfer orbit than the apogee motor can place in circular synchronous equatorial orbit. Therefore, an unconventional trajectory is required to lower the ΔV required of the apogee burn.

The ΔV required of the apogee motor is reduced by decreasing each of the two components which together make up the total ΔV—that needed to circularize the orbit and to reduce the inclination to zero. The ΔV for circularization is reduced by increasing the horizontal velocity at apogee of the transfer orbit without adding radial velocity, which would have to be removed by the apogee burn. Increasing the horizontal velocity at a fixed apogee radius is equivalent to raising the perigee radius of the transfer orbit—thereby decreasing the ellipticity of the transfer orbit.

The ΔV required at apogee for reducing the inclination to zero is decreased by lowering the inclination of the transfer orbit. However, raising the velocity at apogee increases the ΔV required for inclination removal at a fixed transfer orbit inclination. Therefore, the combination of the two methods represents a compromise which is optimized as part of the total problem.

In order to obtain the modified transfer orbit, the trajectory to insertion into that orbit is modified. Most of the inclination reduction is performed by the second burn near the equator, with only a small part of the inclination change accomplished in the ascent to parking orbit.

The characteristics of the optimum parking orbit are changed from the conventional profile to increase the perigee radius of the transfer orbit. An elliptical rather than circular parking orbit is used to raise the altitude of the second burn. The perigee radius of the optimum parking orbit remains limited by aerodynamic heating considerations at some acceptable value. Since injection into the parking orbit occurs near perigee, the vehicle must coast along the ellipse to a higher radius. Because of limitation of the coast duration for the ATS-E mission, the second burn was required to occur near the first equator crossing. [From tracking or other considerations, a second (or greater) equator crossing could be chosen for the second burn, which would increase the parking orbit coast time by a half period (or more).] The latitude of the second burn is no longer equatorial as in the conventional case since the optimum position for raising the perigee radius and decreasing the inclination is dependent on radius and velocity as well as latitude. The parking orbit coast time is greater for this conventional profile since the time to the equator is greater for an elliptical than for a circular parking orbit and additionally, the second burn occurs significantly south of the equator. Optimum true anomalies are found for the beginning and end of the parking and transfer orbit coasts. In addition, the optimum combination of the changes just described as characterizing the unconventional profile is selected.

The desired final inclination for the ATS-E mission is not exactly zero. The perturbations of the sun, moon, and oblateness of the Earth cause a spacecraft to drift from an exactly equatorial orbit. Since zero inclination is not a stable condition, a final orbit inclination yielding the smallest average inclination over the lifetime of the spacecraft is desired. Small final inclinations with the proper inertial ascending node are found to yield acceptable inclination over the lifetime of the satellite. The particular combinations of final orbit inclination and ascending node are functions of the positions of the sun and moon, which are in turn functions of launch time and date. Therefore, payload capability was obtained as a function of final inclination. Negative inclinations are included in the data. This convention indicates that the node has been switched approximately 180° by the apogee burn.

The Altas-Centaur has a 25 min limitation on parking orbit coast time for the mission. Therefore, inclusion of that constraint is necessary for realistic determination of vehicle capability. However, optimizing the coast time provides a more dramatic and obvious demonstration of the optimization procedure. Launch azimuth was not optimized along with the other trajectory parameters, but was investigated parametrically to determine its effect on separated spacecraft mass.

Figure 3 presents separated spacecraft mass as a function of launch azimuth for final inclinations of (−)2° and 5.25° for both optimum and 25 min parking orbit coast times. Separated spacecraft mass is the mass of the spacecraft when it is separated from the Centaur vehicle. This figure shows that the separated spacecraft mass is rather insensitive to launch azimuth. Hence, for simplicity, launch azimuth is fixed at 90° for the remaining figures.

Figure 4a shows the separated spacecraft mass as a function of final inclination. The separated spacecraft mass decreases as final inclination decreases. Figures 4b and 4c show the effect of final inclination on the transfer orbit inclination and inertial velocity at apogee. As might be expected, as the final inclination decreases, so does the transfer orbit inclination.

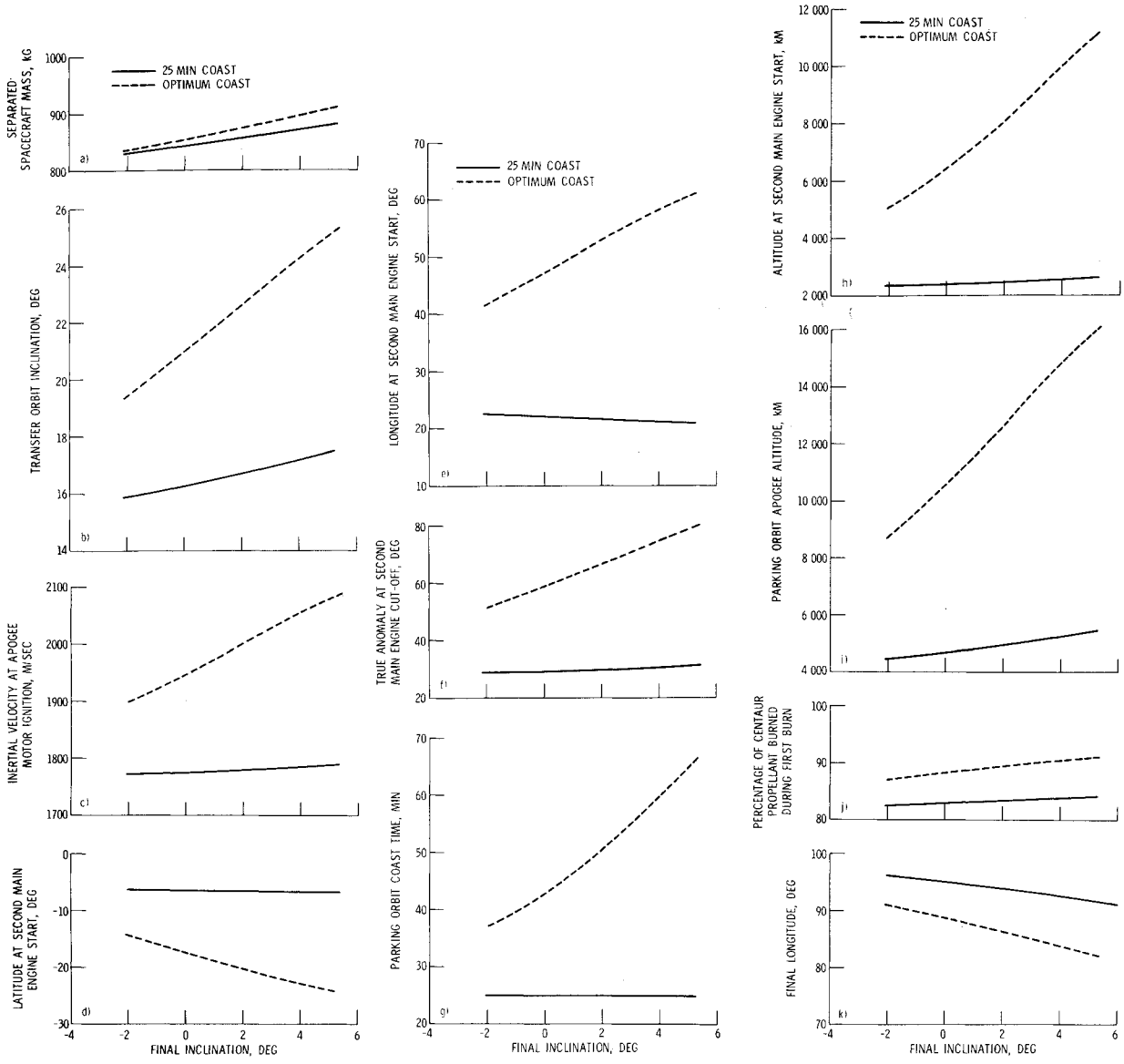

Fig. 4 Various parameters as functions of final inclination.

As might not be expected, the velocity at apogee also decreases as final inclination decreases. Figure 4c–4i show why this occurs. Figure 4d shows the latitude of the second Centaur engine start as a function of final inclination. Since the second burn is required to remove more inclination as final inclination decreases, it is advantageous to move the burn nearer the equator for more efficient plane change. Figure 4e shows that the longitude of second burn start also decreases as final inclination decreases. These trends decrease the parking orbit coast arc as final inclination decreases. This is reflected in a decrease in the true anomaly at second Centaur cutoff, as seen in Fig. 4f. Figures 4g–4i also show additional effects of moving the second burn nearer the equator. It decreases the parking orbit coast time, altitude of the second burn, and the apogee altitude of the parking orbit. These all occur as a result of the decrease in parking orbit coast arc. These figures show why the apogee velocity is decreasing as final inclination decreases. The perigee radius of the transfer orbit decreases as the altitude of the second burn decreases. The apogee altitude of the transfer orbit is almost constant at synchronous altitude, hence as perigee decreases, so does apogee velocity.

Figures 4b and 4c also indicate that more ΔV is required of the apogee motor as final inclination decreases. It can be seen that both the plane change and circularization ΔV are increasing. However, Fig. 4a shows that the ignition mass of the fixed solid motor is decreasing, which increases the ΔV capability of the apogee motor.

Figure 4j shows the percentage of the Centaur propellant used in the first burn. The figure shows that as the final inclination increases, the first burn duration increases as the apogee altitude increases (Fig. 4i).

The final longitude as a function of final inclination is shown in Fig. 4k. It shows that longitude decreases as final inclination increases. The satellite remains at the longitude indicated only when the inclination is zero, the orbit circular, and the altitude synchronous. For other inclinations, the position (latitude and longitude) of the satellite subpoint describes a figure eight on the surface of the rotating Earth. The longitudes indicated in Fig. 4k are injection longitudes, not necessarily the longitude at which the equator crossing occurs. For small inclinations, the longitude does not vary greatly during the period of the orbit.

Now consider the limitation of parking orbit coast time. The 25 min is less than optimum for all the final inclinations considered, as seen in Fig. 4g. The differences in separated spacecraft mass are shown in Fig. 4a. As seen from these figures, as the difference between the optimum and limited coast times decreases, the loss in payload because of the coast time limitation decreases also.

The coast time limitation reduces the advantage of raising the apogee of the parking orbit as final inclination increases. The energy required to raise apogee does not yield the payload increases available with optimum coast time since the altitude cannot be acquired as efficiently in the shorter coast time. The energy is better spent by the second burn to reduce the inclination of the transfer orbit. This is reflected in several of the figures. In Fig. 4b, the transfer orbit inclination for the coast limited case lies well below the optimum case. The lower second burn altitude is reflected in the lower velocity at apogee of the transfer orbit, as seen in Fig. 4c. Because the parking orbit characteristics do not vary greatly with final inclination, the latitude and longitude of the second burn and the true anomaly at second Centaur cutoff are nearly constant. These may be seen in Figs. 4d-4f. The conclusions which may be drawn for the percentage of Centaur propellant used in the first burn and final longitude (Figs. 4j and k), are similar to those for the optimum coast case.

Conclusions

The optimum trajectory to circular synchronous equatorial orbit for a vehicle combination where the apogee motor is smaller than optimum, such as ATS-E, differs significantly from the conventional trajectory. The optimum trajectory employs an elliptical parking orbit and a nonequatorial second propulsion phase with a large amount of plane change, as well as more subtle deviations from the conventional trajectory.

Most important, the results demonstrate that optimum trajectories to circular synchronous equatorial orbits may be obtained with detailed and hence complicated vehicle models for unconventional (small apogee motor) trajectory profiles. These results may be obtained without resorting to exotic mathematical procedures for solving the two-point boundary value problem. The simple Newton-Raphson iteration scheme with the integrated partial derivatives is able to obtain solutions to the highly nonlinear two-point boundary value problem even when the number of initial and final conditions reaches twelve.

Appendix A: Derivation of Optimum Control

The optimization of a trajectory to a circular synchronous equatorial orbit may be considered as the problem of optimizing a multistage launch vehicle to a particular final orbit. The optimization problem to be considered here begins at booster jettison, which is assumed to be a fixed position and velocity. The sustainer portion of the Atlas continues until propellant depletion. The sustainer is jettisoned and a few seconds later the first Centaur burn begins. Its duration is variable and must be optimized. The perigee radius of the parking orbit is fixed. The duration of the parking orbit may or may not be optimized. The parking orbit is not a true coast since a small acceleration is maintained for propellant retention. The duration of the second Centaur burn must be optimized, followed by an optimum transfer orbit coast (a true coast), and a final burn of fixed total impulse. The analysis presented in this Appendix to solve this problem is a special case of the analysis derived in Ref. 3, with an additional constraint—parking orbit perigee radius.

The variational problem to be solved is to find the steering program and various stage durations which maximize the payload capability of a multistage launch vehicle to a specified final orbit. The trajectory must satisfy certain initial, final, and intermediate conditions on the state variables. The thrust, propellant flow rate, and jettison weight for each stage are assumed to be constant. The equations of motion and constraints for each stage may be written as

$$\dot{\mathbf{v}} - \mathbf{G}(\mathbf{r}) - T_i\hat{f}/m = \mathbf{0} \tag{A1a}$$

$$\dot{\mathbf{r}} - \mathbf{v} = \mathbf{0} \tag{A1b}$$

$$\dot{m} + \beta_i = 0 \tag{A1c}$$

$$\hat{f}\cdot\hat{f} - 1 = 0 \tag{A1d}$$

where $\hat{f}$ is the unit thrust direction and $\mathbf{G}(\mathbf{r})$ is the oblate earth gravity acceleration,[6] which may also be written

$$\mathbf{G}(\mathbf{r}) = G_1(r,\mathbf{r}\cdot\hat{z})\hat{r} + G_2(r,\mathbf{r}\cdot\hat{z})\hat{z} \tag{A2}$$

Suppose that each stage of the vehicle is numbered consecutively starting with the booster. For analysis purposes a stage change occurs when the thrust and/or propellant flow rate changes and/or a mass is jettisoned. A Bolza formulation of the variational problem is used,[7] and the functional to be minimized is written as in Ref. 3 as

$$J = -m_f + \sum_{i=2}^{N}\int_{t_{i-1}}^{t_i} F_i dt \tag{A3}$$

where the functional F_i for each stage is

$$F_i = \boldsymbol{\lambda}\cdot[\dot{\mathbf{v}} - \mathbf{G} - T_i\hat{f}/m] + \boldsymbol{\mu}\cdot[\dot{\mathbf{r}} - \mathbf{v}] + \sigma(\dot{m} + \beta_i) + \eta(\hat{f}\cdot\hat{f} - 1) \tag{A4}$$

The resulting Euler-Lagrange equations are

$$\dot{\boldsymbol{\lambda}} + \boldsymbol{\mu} = \mathbf{0} \tag{A5a}$$

$$\dot{\boldsymbol{\mu}} + G_1\boldsymbol{\lambda}/r + (\boldsymbol{\lambda}\cdot\hat{r})\nabla_{\mathbf{r}}G_1 - G_1(\boldsymbol{\lambda}\cdot\hat{r})\hat{r}/r + (\boldsymbol{\lambda}\cdot\hat{z})\nabla_{\mathbf{r}}G_2 = \mathbf{0} \tag{A5b}$$

$$\dot{\sigma} - (T_i/m^2)\boldsymbol{\lambda}\cdot\hat{f} = 0 \tag{A5c}$$

$$2\eta\hat{f} - (T_i/m)\boldsymbol{\lambda} = \mathbf{0} \tag{A5d}$$

The optimum thrust direction $\hat{f}$ is obtained by combining Eqs. (A1d) and (A5d) and using the Weierstrass E-test. This procedure results in

$$\hat{f} = \hat{\boldsymbol{\lambda}} \tag{A6}$$

Since F does not explicitly depend on time, an integral of the motion is

$$C + \boldsymbol{\lambda}\cdot\mathbf{G} + \boldsymbol{\mu}\cdot\mathbf{v} + (T_i/m)\lambda - \sigma\beta_i = 0 \tag{A7}$$

When a spherical gravity model is assumed [i.e., $\mathbf{G}(\mathbf{r}) = G_m^*/r^3\mathbf{r}$], three additional integrals of the motion exist which are given by $\boldsymbol{\lambda}\times\mathbf{v} + \boldsymbol{\mu}\times\mathbf{r} = \text{const}$. Since $\boldsymbol{\lambda}$, $\boldsymbol{\mu}$, $\mathbf{r}$, and $\mathbf{v}$ are all continuous except where an intermediate boundary condition is imposed (as will be shown later), the three integrals are constant across staging points where continuity holds. However, for the oblate gravity model used in this analysis, only a single component of the previous vector integral is constant, as can be verified by differentiation with respect to time.

$$(\boldsymbol{\lambda}\times\mathbf{v} + \boldsymbol{\mu}\times\mathbf{r})\cdot\hat{z} = \text{const} \tag{A8}$$

Transversality Equation

The transversality equation for this problem is

$$dJ = \sum_{i=2}^{N}(C\,dt + \boldsymbol{\lambda}\cdot d\mathbf{v} + \boldsymbol{\mu}\cdot d\mathbf{r} + \sigma\,dm)_{t_{i-1}}^{t_i} - dm_f \tag{A9}$$

which is set equal to zero for an optimal solution. Reference 3 shows that 1) $\boldsymbol{\lambda}$ and $\boldsymbol{\mu}$ are continuous everywhere if there are no intermediate boundary conditions. If the intermediate boundary condition (assumed to occur at a staging point) is expressed as

$$r_p - r_{p,d} = 0 \tag{A10}$$

Reference 8 shows that the discontinuities in $\boldsymbol{\lambda}$ and $\boldsymbol{\mu}$ are $\epsilon\nabla_{\mathbf{v}}r_p$ and $\epsilon\nabla_{\mathbf{r}}r_p$, respectively. The variable ϵ is used as an initial condition in the two-point boundary value problem to satisfy the intermediate boundary condition [Eq. (A10)]. 2) The equations that must be satisfied to optimize the dura-

tion of the powered and coast stages are derived in Ref. 3; the applicable results are presented here. Let j be the first optimized powered stage. Then for constant jettison weight the equation for optimizing stage l is

$$\sum_{i=j}^{l-1} (S_i{}^f - S_{i+1}{}^0) = 0 \tag{A11}$$

where 0 and f refer to initial and final values and the S functions are defined as

$$S_i = C/\beta_i - \sigma = -[\boldsymbol{\lambda}\cdot\mathbf{G} + \boldsymbol{\mu}\cdot\mathbf{v} + (T_i/m)\lambda]/\beta_i, \quad \beta_i \neq 0 \tag{A12a}$$

$$S_i \equiv 0, \ \beta_i = 0 \tag{A12b}$$

where the right side of Eq. (A12a) is obtained by using Eq. (A7). For coasting stages ($\beta_i = T_i = 0$) to be optimized, the equation

$$C_i = (\boldsymbol{\lambda}\cdot\mathbf{G} + \boldsymbol{\mu}\cdot\mathbf{v}) = 0 \tag{A13}$$

must be satisfied for maximum payload. 3) For free initial or final state variable x, the required or final condition for maximum payload (Ref. 4) is

$$\boldsymbol{\lambda}\cdot(\partial\mathbf{v}/\partial x) + \boldsymbol{\mu}\cdot(\partial\mathbf{r}/\partial x) = 0 \tag{A14}$$

If the initial position and velocity are specified, the initial values of any five of the six $\boldsymbol{\lambda}$ and $\boldsymbol{\mu}$ may be used as variable initial conditions in order to satisfy the required final conditions of the two-point boundary value problem. In order to eliminate the difficulty associated with guessing at values of the multipliers, the values of $\boldsymbol{\lambda}$ and $\boldsymbol{\mu}$ can be expressed in terms of pitch and yaw attitudes (ψ and φ) and rates ($\dot{\psi}$ and $\dot{\varphi}$). These equations may be found in Ref. 4, Appendix C. The values of $\boldsymbol{\lambda}$ and $\boldsymbol{\mu}$ are then calculated from:

$$\boldsymbol{\lambda} = \lambda\hat{\boldsymbol{\lambda}} \tag{A15a}$$

$$\boldsymbol{\mu} = -\lambda\hat{\boldsymbol{\lambda}} - \dot{\lambda}\hat{\boldsymbol{\lambda}} \tag{A15b}$$

The value of λ can be set equal to unity without loss of generality. The initial value of $\dot{\lambda}$ can be calculated in closed form, as will be shown by the following development.

Final Conditions

Final conditions for both the conventional and unconventional synchronous equatorial orbit mission require a circular orbit at synchronous orbit altitude with prescribed inclination. If the required inclination is nonzero, both the longitude of the ascending node and the injection point in the final orbit are free for optimization. As shown in Ref. 4, the corresponding auxiliary variational final conditions are

$$(\boldsymbol{\lambda}\times\mathbf{v} + \boldsymbol{\mu}\times\mathbf{r})\cdot\hat{z} = 0 \tag{A16a}$$

and

$$(\boldsymbol{\lambda}\times\mathbf{v} + \boldsymbol{\mu}\times\mathbf{r})\cdot(\mathbf{r}\times\mathbf{v}) = 0 \tag{A16b}$$

If the desired inclination is zero, Eqs. (A16a) and (A16b) degenerate into one equation (zero inclination is equivalent to two final conditions, $\mathbf{r}\cdot\hat{z} = 0$ and $\mathbf{v}\cdot\hat{z} = 0$), and only Eq. (A16a) must be satisfied.

Since Eq. (A16a) is a constant of the motion [Eq. (A8)], it may be satisfied at the beginning of the trajectory, and used to calculate $\dot{\lambda}$. However, it must first be verified that jump discontinuities in $\boldsymbol{\lambda}$ and $\boldsymbol{\mu}$ at the intermediate boundary point does not change the value of the constant. This requires that

$$(\nabla_{\mathbf{v}} r_p \times \mathbf{v} + \nabla_{\mathbf{r}} r_p \times \mathbf{r})\cdot\hat{z} = 0 \tag{A17}$$

It will be shown later than Eq. (A17) is satisfied.

The calculation of $\dot{\lambda}$ proceeds as follows:

$$(\boldsymbol{\lambda}\times\mathbf{v} + \boldsymbol{\mu}\times\mathbf{r})\cdot\hat{z} = (\lambda\hat{\boldsymbol{\lambda}}\times\mathbf{v})\cdot\hat{z} - (\lambda\dot{\hat{\boldsymbol{\lambda}}}\times\mathbf{r})\cdot\hat{z} - (\dot{\lambda}\hat{\boldsymbol{\lambda}}\times\mathbf{r})\cdot\hat{z} = 0 \tag{A18}$$

$$\dot{\lambda} = \lambda(\hat{\boldsymbol{\lambda}}\times\mathbf{v} - \dot{\hat{\boldsymbol{\lambda}}}\times\mathbf{r})\cdot\hat{z}/[(\hat{\boldsymbol{\lambda}}\times\mathbf{r})\cdot z]$$

Computing $\dot{\lambda}$ with Eq. (A18) guarantees that Eq. (A16a) will be satisfied.

Intermediate Conditions

As explained earlier, it is necessary to constrain the perigee radius at injection into the first parking orbit. Otherwise, the optimum solution would result in the parking orbit injection and/or the equator crossing occurring at very low altitudes, thus, violating spacecraft heating constraints. Therefore, the intermediate constraint is given by Eq. (A10), where the desired value corresponds to the perigee altitude.

The required gradients are calculated to be

$$\nabla_{\mathbf{v}} r_p = h(\hat{h}\times\mathbf{r} - r_p{}^2\mathbf{v})/eG_m{}^* \tag{A19a}$$

$$\nabla_{\mathbf{r}} r_p = [(h/G_m{}^*)(\mathbf{v}\times\hat{h}) - r(r_p{}^2/r^2)]/e \tag{A19b}$$

It is easily shown that Eq. (A17) is satisfied for the gradients in Eq. (A19a) and (A19b). Hence the value of $\boldsymbol{\lambda}\times\mathbf{v} + \boldsymbol{\mu}\times\mathbf{r}$ is unaffected by the jump in $\boldsymbol{\lambda}$ and $\boldsymbol{\mu}$.

Boundary Value Problem

For the ATS-E mission, both fixed and optimum parking orbit coast times were considered. The transfer orbit coast time was always optimized, however, along with the durations of the first and second Centaur burns. Based on the preceding discussion of the transversality equation, the initial and and final conditions for the two point boundary value problem are shown in Table 1 for the case where the parking orbit coast time was optimized.

If the desired final inclination is nonzero, then $(\mathbf{r}\cdot\hat{z})$ and $(\mathbf{v}\cdot\hat{z}) = 0$ are replaced by i_d and $(\boldsymbol{\mu}\times\mathbf{r} + \boldsymbol{\lambda}\times\mathbf{v})\cdot(\mathbf{r}\times\mathbf{v}) = 0$. If the parking orbit coast time is fixed, then an initial and final condition are removed. These are t_k and

$$\sum_{i=j}^{k-1} (S_i{}^f - S_{i+1}{}^0) = 0$$

It should be recognized that there may be any number of fixed stages between t_j and t_k, etc. Also, the last three final conditions are evaluated at intermediate points in the trajectory.

Appendix B: Two-Point Boundary Value Problem

The following technique was devised to systematically proceed from a simple, easily converged problem to the solution of the two point boundary value problem for a circular synchronous equatorial orbit.

Table 1 Initial and final conditions

Initial conditions	Final conditions
ψ	E_d
$\dot{\psi}$	r_d
φ	$\dot{r}_d$
$\dot{\varphi}$	$r_{p,d}$ (parking orbit)
ϵ	$(\mathbf{r}\cdot\hat{z}) = 0$
t_j (first Centaur burn)	$(\mathbf{v}\cdot\hat{z}) = 0$
t_k (parking orbit coast)	$\sum_{i=j}^{k-1} (S_i{}^f - S_{i+1}{}^0) = 0$
t_l (second Centaur burn)	$\sum_{i=j}^{l-1} (S_i{}^f - S_{i+1}{}^0) = 0$
t_m (transfer orbit coast)	$(\boldsymbol{\lambda}\cdot\mathbf{G} + \boldsymbol{\mu}\cdot\mathbf{v}) = 0$

A trajectory is obtained to a slightly elliptical (parking) orbit with the desired perigee radius without plane change with a 90° launch azimuth. This problem converges easily. Then the ascent burn time is fixed at the value obtained and a variable length parking orbit coast, a fixed parking orbit perigee radius and second burn are added. This problem is targeted to the desired apogee and 180° argument of perigee for first equator crossing second burn. An inclination decrease of about two degrees is then added to these final conditions and the problem is retargeted to the augmented final conditions. Now the transfer orbit coast (variable) and apogee burn (fixed or variable) are added. This trajectory is integrated to the end with the converged initial guesses from the last step. The final conditions achieved will frequently be far from a circular synchronous equatorial orbit. However, specify the final conditions actually achieved as the desired ones, and optimize the problem. The parking orbit coast, second burn, and transfer orbit coast durations will change. Now alter the achieved final conditions toward the desired ones judiciously in steps, retargeting at each step. In this manner, the desired final orbit conditions may be obtained. Now the ascent burn duration may be optimized. Any sizable change in a constraint or final condition is best achieved by proceeding in steps. The problem is quite nonlinear. Attempts to plot initial conditions as functions of the final conditions for extrapolation purposes were made. They were generally unsuccessful.

References

[1] Hoelker, R. F. and Silber, R., "Injection Schemes for Obtaining a Twenty-Four Hour Orbit," *Aerospace Engineering*, Vol. 20, No. 1, Jan. 1961, pp. 28–29, 76–84.

[2] Rider, L., "Characteristic Velocity Requirements for Impulsive Thrust Transfers Between Non Co-Planar Circular Orbits," *ARS Journal*, Vol. 31, No. 3, March 1961, pp. 345–351.

[3] Teren, F. and Spurlock, O. F., "Payload Optimization of Multi-stage Launch Vehicles," TN D-3191, 1966, NASA.

[4] Teren, F. and Spurlock, O. F., "Optimal Three Dimensional Launch Vehicle Trajectories with Attitude and Attitude Rate Constraints," TN D-5117, 1969, NASA.

[5] Spurlock, O. F. and Teren, F., "A Trajectory Code for Maximizing the Payload of Multistage Launch Vehicles," TN D-4729, 1968, NASA.

[6] Clarke, V. C., Jr., "Constants and Related Data Used in Trajectory Calculations at the Jet Propulsion Laboratory," JPL-TR-32-273, May 1962, Jet Propulsion Lab., California Inst. of Technology, Pasadena, Calif.

[7] Bliss, G. A., *Lectures on the Calculus of Variations*, University of Chicago Press, Chicago, Ill., 1946.

[8] Pontryagin, L. S. et al., *The Mathematical Theory of Optimal Processes*, Interscience, New York, 1962.

[9] Dobson, W. F., Huff, V. N., and Zimmerman, A. V., "Elements and Parameters of the Osculating Orbit and Their Derivatives," TN D-1106, 1962, NASA.

DECEMBER 1971 J. SPACECRAFT VOL. 8, NO. 12

The Critical Dynamic Errors of a Strapdown Guidance System

D. SARGENT* AND H. ZARETT†
TRW Systems, Redondo Beach, Calif.

Strapdown inertial guidance systems have their sensors fixed to the body of the guided vehicle. The system is subjected to vehicle dynamic environments (limit cycle and vibration). Simulations and analyses of one such strapdown system, the Apollo LM Abort Guidance System, were performed to model dynamic errors. There resulted three critical dynamic errors: gyro asymmetry, wheel speed modulation, and coning. The analytic models for these error sources were then verified by test. Dynamic error magnitude predictions were made and implemented into an overall system error model. These predictions were compared to flight results as encountered on the LM lunar mission.

Nomenclature

$A(\Omega_x)$ = gyro loop asymmetry, a function of Ω_x
AGS = Abort Guidance System
ASA = Abort Sensor Assembly, the AGS subassembly containing the sensors and associated electronics
$B(f)$ = computer attenuation function for coning
CSD = cross spectral density
E = "expected value of"
f, f_s = frequency and computer sampling frequency, Hz
$F_1(s), F_2(s)$ = WSM transfer functions
$G_i(s)$ = frequency response of the ith gyro loop
H = gyro wheel angular momentum (2.5×10^5 dyne-cm-sec for AGS)
i,j,k = cyclic permutations of the subscripts, or superscripts, X, Y, and Z
Im = "imaginary part of"
J = gyro float moment of inertia about the output axes, 354 gm-cm² for AGS
LM = Lunar Module
$N(\Omega_x)$ = gyro loop nonlinearity
PGNCS = Primary Guidance, Navigation, and Control System of the LM
PSD = power spectral density
$p(\Omega_x)$ = probability density function of Ω_x
$P_{LC}(\Omega_x)$ = probability density function of the limit cycle part of Ω_x
$p_v(\Omega_x)$ = probability density function of the random vibrational part of Ω_x
PWM = pulse width modulated
RCS = reaction control system
Re = "real part of"
S = Laplace operator, also $S = j\omega = j2\pi f$
SIMU = strapdown inertial measuring unit
SMRD = spin motor rotation detector
T = period of a square wave
TDM = time domain multiplication
WSM = wheel speed modulation
$Y(\Omega_x)$ = gyro loop output including the nonlinearity
α = coning angle

Presented as Paper 70-1029 at the AIAA Guidance, Control and Flight Mechanics Conference, Santa Barbara, Calif., August 17–19, 1970; submitted September 18, 1970; revision received June 3, 1971.

* Section Head.
† Group Leader.